

Coupled piezo-elastodynamic modeling of guided wave excitation and propagation in plates with applied prestresses

F. Song¹, G. L. Huang¹ and G. K. Hu²

Journal of Intelligent Material Systems
and Structures

24(5) 598–611

© The Author(s) 2012

Reprints and permissions:

sagepub.co.uk/journalsPermissions.nav

DOI: 10.1177/1045389X12467516

jim.sagepub.com



Abstract

Plate-like aerospace engineering structures are prone to mechanical/residual preloads during flight operation. This article focuses on the quantitative characterization of applied prestress effects on the piezoelectrically-induced guided wave propagation, which has been widely used in structural health monitoring systems. An analytical model considering coupled piezo-elastodynamics is developed to study dynamic load transfer between a surface-bonded thin piezoelectric actuator and a prestressed plate. The accuracy of the analytical prediction is evaluated by the comparison with the finite element analysis. Based on the developed model, the load-dependent guided wave signal variation in both time-of-flight and amplitude is determined, and its dependence on loading frequency and host material properties is also discussed. It is found that the guided wave signal variation due to the prestress could be significant under some circumstances. A signal difference coefficient is finally proposed to quantitatively assess the signal variation caused by different prestresses. This study can serve as a theoretical foundation for the development of the real-time piezo-guided wave-based structural health monitoring system in a realistic loading environment.

Keywords

Piezo-elastodynamic modeling, dynamic load transfer, guided wave generation, prestress/residual stress, guided wave-based structural health monitoring

Introduction

Ultrasonic guided waves (GWs), which can propagate over large distances in plates and shells, have shown great potential for structural health monitoring (SHM) of thin-walled aircraft and aerospace structures over the past decades (Anton et al., 2009; Kundu and Maslov, 1997; Senesi and Ruzzene, 2011; Song et al., 2012). Due to advantages such as quick response, low power consumption, low cost, and small size, piezoelectric wafers are particularly suitable for being integrated in those structures as actuators/sensors to form an active on-line SHM system (Giurgiutiu, 2005; Ihn and Chang, 2008; Park et al., 2010; Raghavan and Cesnik, 2007; Song et al., 2009). Many damage diagnosis and characterization approaches have been developed and suggested by comparing the GW signals from the damaged structures to the baselines recorded from the undamaged structures (Huang et al., 2010b; Lin and Yuan, 2005; Michaels, 2008). However, implementation of those approaches are mostly based on the condition that the monitored structures are under the ideal

laboratory environment, in which the working loads on the monitored structures such as mechanical/residual prestresses are not considered.

It is well known that operating aircraft and aerospace structures are often subjected to various prestresses such as applied loads. During manufacture and assembly, many load-bearing elements of aircraft such as fuselages, longerons, stringers, bulkheads, and stabilizers are fully or partially prestressed to enhance their fatigue strength and fracture resistance (Ratwani, 2000). In bolted aerospace structures, applied stresses can be exerted by the bolts on the surrounding material of the joints (Doyle et al., 2010). Significant thermal

¹Department of Systems Engineering, University of Arkansas at Little Rock, Little Rock, AR, USA

²School of Aerospace Engineering, Beijing Institute of Technology, Beijing, China

Corresponding author:

G. L. Huang, Department of Systems Engineering, University of Arkansas at Little Rock, 2801 S University Avenue, Little Rock, AR 72204, USA.
Email: glhuang@ualr.edu

residual stresses in aerospace composite structures can be initiated due to the difference in thermal expansion coefficient (CTE) and mechanical incompatibility of the different components when the structures serve under extreme temperature environment (Karami et al., 2008). Thin-walled aerospace structures are usually operated under in-plane loads during flight service. For instance, spinning helicopter rotor blades, bladed disks in engines, and pressurized aircraft cabins are under tensile loads while buoyant structures are under compressive loads due to gravitational forces or pressure loads (Lesieutre, 2009). Therefore, consideration of prestress effects on the GW excitation and propagation in thin-walled aerospace structures is of practical importance in the design of an in situ SHM system.

A number of research activities have been conducted on characterization of mechanical and dynamic behaviors of various prestressed structures (Akbarov, 2007; Hu et al., 2002; Kwun et al., 1998; Loveday, 2009; Singh, 2010; Tiersten et al., 1981; Yang, 2005) by using analytical, numerical, or experimental methods. Desmet et al. (1996) studied effects of the externally applied stress on the fundamental Lamb wave propagation in polymer foils. It was found that the applied tensile stress had very small influence on the dispersion of the symmetric mode compared to the antisymmetric mode. Based on the finite element modeling, Chen and Wilcox (2007) examined pretension influences on the GW propagation in cables and rails, and found that the wave velocity of the fundamental flexural wave changed significantly due to the appearance of tensile load, especially for low-frequency cases. An and Sohn (2010) tested the transient GW responses in plates under various static loading conditions and similar conclusions were drawn. Doyle et al. (2010) and Zagrai et al. (2010) experimentally studied the acoustoelastic effects of piezoelectric wafer-active sensors (PWAS) bonded onto the bolted space structures under different prestresses. Recently, the effects of applied loads on GW responses were experimentally investigated in the context of environmental load impacts on GW-based SHM using piezoelectric wafers (Michaels et al., 2011). To the best of our knowledge, however, no systematic theoretical study has been carried out to quantitatively characterize prestress effects on the coupled piezo-elastodynamic behavior of surface-bonded piezoelectric wafers. Such theoretical framework would be fundamental in understanding the reliability and feasibility of applying piezo-GW-based SHM systems for field applications.

Based on the Bernoulli–Euler beam theory, Crawley and De Luis (1987) developed a static shear-lag model to study the interfacial load transfer between a piezo-actuator and a substructural coupled beam for low-frequency cases. A direct extension of the classical shear-lag theory (Crawley and De Luis, 1987) has been reported (Giurgiutiu and Santoni, 2009), where the nonlinear stress distribution across the thickness was

considered. To avoid the difficulties associated with the complex interaction between the actuator and the host medium, the interfacial shear stress was simplified as “pinching” tangential traction only at the actuator tips on the structure surface by neglecting coupled actuator/structural dynamics (Raghavan and Cesnik, 2005; Von Ende and Lammering, 2007). To consider the coupled piezo-elastodynamic behavior, a one-dimensional actuator model has been developed to investigate the coupled dynamic load transfer between the piezo-actuator and the semi-infinite elastic medium (Huang et al., 2010b; Huang and Sun, 2006; Wang and Huang, 2001). Similarly, an integral equation-based model was also proposed to study the patch–layer interaction and resonance effects in a system of flexible piezoelectric patch actuators bonded to an elastic substrate (Glushkov et al., 2007). However, the piezo-actuator model surface bonded to a prestressed plate structure has not been developed.

In this article, we extend the one-dimensional actuator model (Huang and Sun, 2006; Wang and Huang, 2001) to quantitatively investigate the interfacial shear stress and its resulting GW propagation in the prestressed isotropic plate. The interfacial shear stress between the actuator and the host plate is calculated using the Fourier transform technique and solving the resulting integral equations. The analytical predictions of the interfacial shear stress and transient responses from the current model are compared with the finite element simulation results to evaluate the accuracy of the developed model. Based on the current model and the modified Rayleigh–Lamb equations in the prestressed plate, the load-dependent GW excitation and propagation by the piezoelectric wafer actuator is studied, from which the prestress effects are demonstrated. It is found that the wave response variation induced by the prestresses could be significant under some circumstances, which is quantitatively characterized by a proposed signal difference coefficient (SDC).

Formulation of the problem

Consider a plane strain problem of a thin piezo-actuator surface bonded to an isotropic host plate subjected to a uniform prestress, as sketched in Figure 1. In this figure, the half-length and the thickness of the actuator are denoted as a and h , respectively, and the half-thickness of the host plate is d . The host plate is under a uniaxial static prestress σ^0 along the x direction. The poling direction of the actuator is along the z -axis, and a voltage (ΔV) between the upper and lower electrodes of the actuator is then applied, which results in an electrical field (E_z) of circular frequency ω along the poling direction of the actuator. For the steady-state harmonic solution of the system, the time factor $\exp(-i\omega t)$, which applies to all the field variables, is

suppressed in the following analysis. In the current model, it is assumed that the piezo-actuator is bonded onto the substructure after manufacturing. Conceptually, this is an ideal assumption for the achievement of online SHM based on surface-bonded piezo-wafers (Giurgiutiu, 2008). Under this conceptual assumption, our model is mainly for considering the effects of applied prestresses (during operation) on piezo-actuated GWs. The perfect actuator/structure bonding is assumed in the current model and the adhesive interface layer effects (Dugnani, 2009; Han et al., 2009; Jin and Wang, 2011; Lanza di Scalea and Salamone, 2008) are neglected.

Modeling of the prestressed piezoelectric actuator

In this study, attention is paid to modeling the thin actuator, for which the thickness is very small compared with its length. In response to an electric field (E_z) applied across its thickness along the poling direction, the actuator mainly experiences axial deformation. Therefore, the prestressed actuator can be modeled as an electroelastic element subject to the applied electric field and the distributed interfacial stress, as illustrated in Figure 2. In this figure, $\hat{\sigma}^0$ is the resulting initial stress in the actuator due to the prestress σ^0 on the host plate, and τ represents the interfacial shear stress transferred between the actuator and the host plate.

It is assumed that the incremental stress σ_x^a and displacement u_x^a are uniform across the actuator. Under plane strain deformation, the axial incremental stress in the actuator (σ_x^a) can be expressed as

$$\sigma_x^a = E_a \varepsilon_x^a - e_a E_z \quad (1)$$

where E_a and e_a are the effective elastic and piezoelectric material constants, $E_a = c_{11} - c_{13}^2/c_{33}$ and $e_a = e_{13} - e_{33}c_{13}/c_{33}$, respectively, and $E_z = -\Delta V/h$ with c_{ij} and e_{ij} ($i, j = 1, 3$, or x, z) being the components of the piezoelectric elastic stiffness matrix for a constant electric potential, and the piezoelectric constant matrix, respectively. The small strain component is given by

$$\varepsilon_x^a = \frac{du_x^a}{dx} \quad (2)$$

By considering the incremental deformation (Su et al., 2005) together with equations (1) and (2), the equation of motion of the prestressed actuator can be written as

$$[E_a + \hat{\sigma}_{ave}^0] \frac{d^2 u_x^a}{dx^2} + \frac{\tau(x)}{h} + \rho_a \omega^2 u_x^a = 0 \quad (3)$$

where ρ_a is the mass density of the actuator, and $\hat{\sigma}_{ave}^0 = 1/2a \int_0^{2a} \hat{\sigma}^0(x) dx$ is an averaged resulting stress over the actuator length for simplification of the problem. The determination of the resulting initial stress $\hat{\sigma}^0(x)$ can be found in Appendix 1. Since the load transferred between the actuator and the host plate can be attributed to τ , two ends of the actuator during incremental deformation can be assumed as

$$\sigma_x^a = 0, \quad |x| = a \quad (4)$$

The axial strain of the actuator can be obtained in terms of the interfacial shear stress τ by solving equation (3) as

$$\varepsilon_x^a = \varepsilon_E(x) + \frac{\sin k_a(a+x)}{h(E_a + \hat{\sigma}_{ave}^0) \sin 2k_a a} \int_{-a}^a \cos k_a(\zeta - a) \tau(\zeta) d\zeta - \int_{-a}^y \cos k_a(\zeta - x) \frac{\tau(\zeta)}{h(E_a + \hat{\sigma}_{ave}^0)} d\zeta \quad (5)$$

where $\varepsilon_E(x) = (e_a E_z / (E_a + \hat{\sigma}_{ave}^0)) (\cos k_a x / \cos k_a a)$, $k_a = \omega / c_a$, and $c_a = ((E_a + \hat{\sigma}_{ave}^0) / \rho_a)^{1/2}$ with k_a and c_a being the wave number and the axial wave velocity of the prestressed actuator, respectively.

GW solution of the prestressed plate structure

Under the plane strain deformation, the elastic wave motion for a prestressed material can be expressed as follows (Akbarov, 2007; Liu et al., 2003; Wang et al., 2007)

$$\nabla^2 \varphi + \left(\frac{\sigma^0}{\lambda + 2\mu} \right) \frac{\partial^2 \varphi}{\partial x^2} + \frac{\omega^2}{c_l^2} \varphi = 0 \quad (6)$$

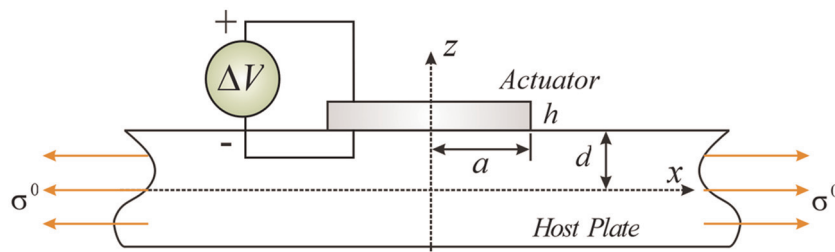


Figure 1. An actuator surface-bonded to an elastic plate under the static prestress.

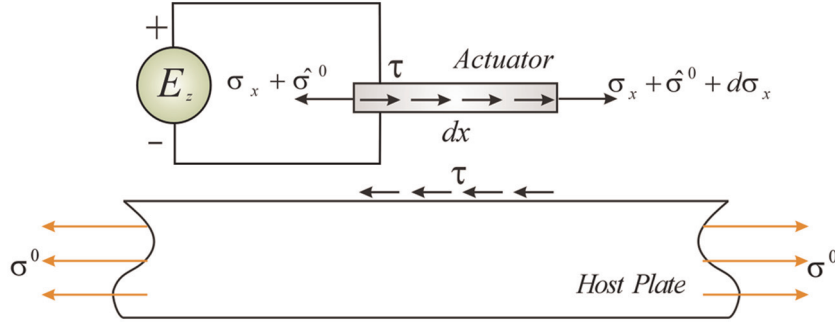


Figure 2. The schematic diagram of the actuator model.

$$\nabla^2 \psi + \left(\frac{\sigma^0}{\mu} \right) \frac{\partial^2 \psi}{\partial x^2} + \frac{\omega^2}{c_t^2} \psi = 0 \quad (7)$$

where ρ is the mass density of the host medium, $c_t^2 = (\lambda + 2\mu)/\rho$, and $c_l^2 = \mu/\rho$ with λ and μ being the Lamé constants, respectively, and φ and ψ are the two displacement potentials that satisfy the following equation

$$u_x = \frac{\partial \varphi}{\partial x} + \frac{\partial \psi}{\partial z} \quad \text{and} \quad u_z = \frac{\partial \varphi}{\partial z} - \frac{\partial \psi}{\partial x} \quad (8)$$

The general solution of the wave propagation can be determined by solving equations (6) and (7) using the spatial Fourier transform as follows

$$\bar{\phi}(\xi) = \int_{-\infty}^{+\infty} \phi(x) e^{i\xi x} dx \quad \text{and} \quad \phi(x) = \frac{1}{2\pi} \int_{-\infty}^{+\infty} \bar{\phi}(\xi) e^{-i\xi x} d\xi \quad (9)$$

The solutions can be expressed as follows

$$\bar{\varphi} = A_1 \sin(pz) + A_2 \cos(pz) \quad (10)$$

$$\bar{\psi} = B_1 \sin(qz) + B_2 \cos(qz) \quad (11)$$

where $p^2 = (\omega^2/c_l^2) - (1 + (\sigma^0/(\lambda + 2\mu)))\xi^2$ and $q^2 = (\omega^2/c_t^2) - (1 + (\sigma^0/\mu))\xi^2$. Using the linear strain–displacement relation and the constitutive equation, the stresses can be readily determined as

$$\bar{\sigma}_{zz} = \mu \begin{bmatrix} (\xi^2 - q^2) \sin(pz) A_1 + (\xi^2 - q^2) \cos(pz) A_2 \\ -2\xi q \cos(qz) i B_1 + 2\xi q \sin(qz) i B_2 \end{bmatrix} \quad (12)$$

$$\bar{\sigma}_{xz} = \mu \begin{bmatrix} 2\xi p \cos(pz) i A_1 - 2\xi p \sin(pz) i A_2 \\ + (\xi^2 - q^2) \sin(qz) B_1 + (\xi^2 - q^2) \cos(qz) B_2 \end{bmatrix} \quad (13)$$

Based on the present actuator model, the boundary condition on the upper surface of the host plate can be written as

$$\sigma_{xz}(x, d) = -\tau(x), \quad |x| < a \quad \text{and} \quad \sigma_{zz}(x, d) = 0 \quad (14)$$

Using equations (12)–(14) and applying the inverse Fourier transform, the Lamb strain component ε_x on

the surface $z = d$ can be expressed in terms of the interfacial shear stress τ as follows

$$\varepsilon_x(x, d) = -\frac{1}{4\pi\mu} \int_{-\infty}^{+\infty} \tau(\eta) \int_{-\infty}^{+\infty} i \left[\frac{N_S(\xi)}{D_S(\xi)} + \frac{N_A(\xi)}{D_A(\xi)} \right] e^{-i\xi(x-\eta)} d\xi d\eta \quad (15)$$

in which $N_S(\xi) = \xi q \cos(pd) \cos(qd) (\xi^2 + q^2)$, $D_S(\xi) = (\xi^2 - q^2)^2 \cos(pd) \sin(qd) + 4\xi^2 pq \sin(pd) \cos(qd)$, $N_A(\xi) = -\xi q \sin(pd) \sin(qd) (\xi^2 + q^2)$, and $D_A(\xi) = (\xi^2 - q^2)^2 \sin(pd) \cos(qd) + 4\xi^2 pq \cos(pd) \sin(qd)$

The integral in equation (15) is singular at the roots of D_S and D_A , which represent the symmetric and antisymmetric eigenvalues of the modified Rayleigh–Lamb equations at frequency ω with the prestress parameter σ^0 . At low frequencies, only two eigenvalues ξ_0^S and ξ_0^A exist, while several eigenvalues appear at sufficiently high frequencies. For $\sigma^0 = 0$, the dispersion equations can be reduced to the conventional Rayleigh–Lamb equations without load (Raghavan and Cesnik, 2005).

Dynamic load transfer and resulting GW propagation

The continuity between the actuator and the host plate at $z = d$ can be described as

$$\varepsilon_x^a(x) = \varepsilon_x(x, d), \quad |x| < a \quad (16)$$

By substituting equations (5) and (15) into equation (16), the integral equation can be obtained as

$$\begin{aligned} & -\frac{1}{4\pi\mu} \int_{-\infty}^{+\infty} \tau(\eta) \int_{-\infty}^{+\infty} i \left[\frac{N_S(\xi)}{D_S(\xi)} + \frac{N_A(\xi)}{D_A(\xi)} \right] e^{-i\xi(x-\eta)} d\xi d\eta \\ & - \frac{\sin k_a(a+x)}{h(E_a + \hat{\sigma}_{ave}^0) \sin 2k_a a} \int_{-a}^a \cos k_a(\zeta - a) \tau(\zeta) d\zeta \\ & + \int_{-a}^x \cos k_a(\zeta - x) \frac{\tau(\zeta)}{h(E_a + \hat{\sigma}_{ave}^0)} d\zeta = \frac{e_a E_z}{(E_a + \hat{\sigma}_{ave}^0)} \frac{\cos k_a x}{\cos k_a a} \end{aligned} \quad (17)$$

Equation (17) is a singular integral equation of the first kind, which involves a square-root singularity of τ at the ends of the actuator. The general solution of τ can be expressed in terms of Chebyshev polynomials, such that

$$\tau(x) = \sum_{j=0}^{+\infty} c_j T_j(x/a) / \sqrt{1 - (x/a)^2} \quad (18)$$

with T_j being Chebyshev polynomials of the first kind.

If the expression in equation (18) is truncated to the N -th term and equation (17) is satisfied at the following collocation points along the length of the actuator

$$x^l = a \cos \left(\frac{l-1}{N-1} \pi \right), \quad l = 1, 2, \dots, N \quad (19)$$

N linear algebraic equations in terms of $\{c\} = \{c_1, c_2, \dots, c_{N-1}\}^T$ can be obtained as

$$[M]\{c\} = \{F\} \quad (20)$$

where $[M]$ is a known matrix given by

$$\begin{aligned} M_{lj} = & -\frac{\nu_0}{2\mu} \sum_{j=1}^{+\infty} c_j \frac{\sin[j\cos^{-1}\bar{x}^l]}{\sin[\cos^{-1}\bar{x}^l]} \\ & + \frac{\nu_0}{2\mu} \sum_{j=1}^{+\infty} c_j \int_0^{+\infty} P_j^l(\bar{\xi}, \bar{x}^l) \left[\frac{N_S(\bar{\xi})}{\nu_0 D_S(\bar{\xi})} + \frac{N_A(\bar{\xi})}{\nu_0 D_A(\bar{\xi})} + 1 \right] d\bar{\xi} \\ & + \frac{a}{h(E_a + \hat{\sigma}_{ave}^0)} \sum_{j=1}^{+\infty} c_j \int_{\cos^{-1}\bar{x}^l}^{\pi} \cos[\bar{k}_a(\cos\theta - \bar{x}^l)] \cos(j\theta) d\theta \\ & + \frac{a\pi}{h(E_a + \hat{\sigma}_{ave}^0)} \frac{\sin[\bar{k}_a(\bar{x}^l + 1)]}{\sin(2\bar{k}_a)} \sum_{j=1}^{+\infty} c_j P_j^2 \end{aligned}$$

with $\nu_0 = 2(1 - \nu)$ (ν is the Poisson's ratio of the host medium),

$$\bar{x}^l = x^l/a, \bar{k}_a = \bar{k}_a a, \bar{\xi} = \xi a,$$

$$P_j^l(\bar{\xi}, \bar{x}^l) = J_j(\bar{\xi}) \begin{cases} (-1)^n \cos(\bar{\xi}\bar{x}^l) & j = 2n + 1 \\ (-1)^{n+1} \sin(\bar{\xi}\bar{x}^l) & j = 2n \end{cases},$$

$$P_j^2 = J_j(\bar{k}_a) \begin{cases} (-1)^n \sin(\bar{k}_a) & j = 2n + 1 \\ (-1)^n \cos(\bar{k}_a) & j = 2n \end{cases}$$

with J_j ($j = 1, 2, \dots$) being the Bessel functions of the first kind, and $\{F\}$ is the applied load with $F_l = \varepsilon_E(x^l)$, $l = 1, 2, \dots, N$. From these equations, the unknown coefficients in $\{c\}$ can be determined, from which the interfacial shear stress τ can be obtained. By applying the residue theorem (Raghavan and Cesnik, 2005) and using the resulting $\{c\}$ in equations (18) and (15), the steady-state Lamb strain induced by the piezo-actuator on the surface $z = d$ can be determined as

$$\varepsilon_x(x, d) = \frac{-\pi i}{2\mu} \sum_{j=1}^N c_j$$

$$\begin{cases} (-1)^n \left[\begin{aligned} & \sum_{\bar{\xi}^S} \frac{N_S(\bar{\xi}^S)}{D_S(\bar{\xi}^S)} J_j(\bar{\xi}^S) \cos(\bar{\xi}^S \bar{x}^l) \\ & + \sum_{\bar{\xi}^A} \frac{N_A(\bar{\xi}^A)}{D_A(\bar{\xi}^A)} J_j(\bar{\xi}^A) \cos(\bar{\xi}^A \bar{x}^l) \end{aligned} \right], & j = 2n + 1 \\ (-1)^{n+1} \left[\begin{aligned} & \sum_{\bar{\xi}^S} \frac{N_S(\bar{\xi}^S)}{D_S(\bar{\xi}^S)} J_j(\bar{\xi}^S) \sin(\bar{\xi}^S \bar{x}^l) \\ & + \sum_{\bar{\xi}^A} \frac{N_A(\bar{\xi}^A)}{D_A(\bar{\xi}^A)} J_j(\bar{\xi}^A) \sin(\bar{\xi}^A \bar{x}^l) \end{aligned} \right], & j = 2n \end{cases} \quad (21)$$

in which $\bar{\xi}^S = \xi^S/a$ and $\bar{\xi}^A = \xi^A/a$. It should be mentioned that while a single circular frequency ω is assumed for harmonic excitation in the above analysis, the transient GW response to any time-limited signal can be evaluated by taking the inverse Fourier transform of the integral of the product of the harmonic response multiplied by the Fourier transform of the excitation signal over the bandwidth (Raghavan and Cesnik, 2005).

Validation of the model

To evaluate the developed model, predictions from the current model will be compared with the results by using commercially available finite element (FE) code ANSYS/Multiphysics 11.0. The two-dimensional PLANE13 element with four nodes and three degrees-of-freedom (DOF) at each node is selected for the piezo-actuator and the plate. The additional DOF in the coupled field element is the electrical voltage. The input voltage can be applied on the top nodes of the piezo-actuator, and zero voltage is assigned for all the bottom nodes of the piezo-actuator to simulate the grounding operation. The material properties of the actuator used for the following numerical examples are given in Table 1.

Static deformation analysis is first conducted to compute the initial interfacial stress distribution between the piezo-actuator and the host plate caused by prestresses. Transient analysis is then performed to calculate the dynamic response of the prestressed plate (Chen and Wilcox, 2007).

Initial interfacial load transfer

First, consider the initial static deformation of the piezo-actuator surface bonded to the prestressed plate. The material properties of the actuator can be found in Table 1, and $E = 2.74 \times 10^{10}$ Pa and $\nu = 0.3$ are used for the host plate (Wang and Huang, 2001). Figure 3

Table 1. Material properties of the piezo-actuator (Wang and Huang, 2001).

c_{11} (10^{10} N/m ²)	c_{13} (10^{10} N/m ²)	c_{33} (10^{10} N/m ²)	e_{31} (C/m ²)	e_{33} (C/m ²)	ρ_a (kg/m ³)
13.9	7.43	11.5	-5.2	15.1	7500

shows the normalized initial static interfacial shear stress distribution between the actuator and the prestressed host plate with varying actuator half-length-to-thickness ratios (a/h). In this figure, $\tau^{0*} = |\tau/\sigma^0|$, $\rho_a/\rho = 1$, and $H/h = 40$ with $H = 2d$ being the plate thickness. In this analysis, 40 terms in Chebyshev polynomial expansions are used. It can be seen that the interfacial shear stress more and more concentrates the actuator tips with the increase of the actuator length-to-thickness ratio, as predicted by both the current model and the FE simulation. Excellent agreement between the current model and the FE simulation is observed especially for the actuator with large length-to-thickness ratios, that is, $a/h > 10$ that validates the applicability of the current one-dimensional actuator model and the averaged resulting stress assumption in the integrated piezo-plate structure.

Transient GW propagation

To further show capability of the developed model, the transient GW signals generated by the piezo-actuator surface bonded to prestressed plates are evaluated in this subsection. The excitation used in the study is a five-peak tone-burst signal (Song et al., 2012), which has been widely used for the GW-based SHM. To obtain the theoretical transient GW response, the inverse Fourier transform of the harmonic solution is conducted over the frequency spectrum of the excited tone-burst signal. Figure 4 shows the normalized transient strain responses predicted by the current model (equation (21)), and the FE model at a central excitation frequency of $f_c = 100$ kHz. The material properties of the actuator are given in Table 1 and the host plate material is assumed to be a typical aircraft-grade aluminum alloy ($E = 79$ GPa, $\nu = 0.33$ and $\rho = 2600$ kgm⁻³) with the yield strength around $\sigma_Y = 0.5$ GPa (Santus and Tayler, 2009), respectively. In Figure 4, Am^* is the normalized surface strain component ε_x with respect to its maximum value. In the example, the applied prestress is $\sigma^0 = 0.8\sigma_Y$, geometry parameters are $a/h = 20$, $H/h = 13.3$ with $H = 2d$, and the strain is calculated at $x = 226.5$ mm away from the actuator. In Figure 4, a complete separation of the fundamental symmetric mode (S0) and antisymmetric mode (A0) can be observed. Specifically, very good agreement in both wave amplitude and phase can be clearly seen between the current model and the FE simulation, which shows the capability of the current model in quantitatively describing the GW excitation and propagation in the prestressed plate.

Effects of prestresses on GW propagation

In this section, attention is paid to characterization of the prestress effects on the GW generation and propagation based on the developed analytical model. In the following calculation, the actuator material properties are listed in Table 1, and the typical aircraft-grade aluminum alloy ($E = 79$ GPa, $\nu = 0.33$ and $\rho = 2600$ kgm⁻³) with the yield strength around $\sigma_Y = 0.5$ GPa (Santus and Tayler, 2009) is considered as the host plate. The static prestresses varying in the range of ± 0.4 GPa are considered, where the positive and negative prestresses physically denote tension and compression, respectively.

Dispersion of the fundamental Lamb wave modes

Figure 5 shows the dispersion curves of the fundamental S0 and A0 Lamb wave modes in the plate under different prestresses. In this figure, c_p and c_t represent the phase velocity of Lamb waves and the transverse bulk wave velocity, respectively, and $f-H$ is the product of frequency and plate thickness. In Figure 5(a), the dispersion properties of the S0 mode show small sensitivity to the applied prestresses throughout all considered frequencies. For instance, the predicted change in the velocity is less than 0.25% for most frequencies even when the stress is applied up to $0.8\sigma_Y$. However, for the A0 mode in Figure 5(b), an obvious shift in the wave velocity can be seen with the change of the applied prestresses especially at relatively low frequencies. It can be found that phase velocities of the A0 mode increase with the increase of tensile stresses and decrease with the increase of compressive stresses. The A0 mode has been widely used to detect various damages in metallic plates due to its high sensitivity to structural damage (Francis Rose and Wang, 2010; Fromme and Sayir, 2002). Therefore, when the A0 mode is used to evaluate the structures under prestressed work conditions, the wave signal variation caused by the prestress should be taken into account. Interestingly, stopping bands of the A0 mode are observed in compressed plates for the relatively low frequencies, which represent evanescent wave propagation.

Figure 6 shows the velocity variation of GW modes in the prestressed plate with different material properties. In this figure, the normalized prestress-induced wave velocity variation is defined as

$$\Delta c^*(\sigma^0) = [c_p(\sigma^0) - c_p(\sigma^0 = 0)]/c_p(\sigma^0 = 0) \quad (22)$$

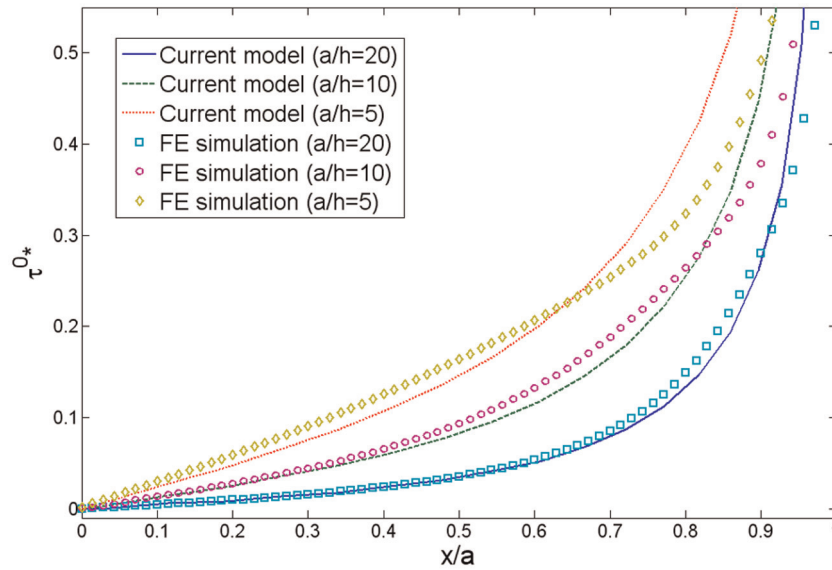


Figure 3. The normalized initial static interfacial shear stress of the piezo-actuator surface-bonded to the prestressed plate with varying actuator half-length-to-thickness ratio a/h . FE: finite element.

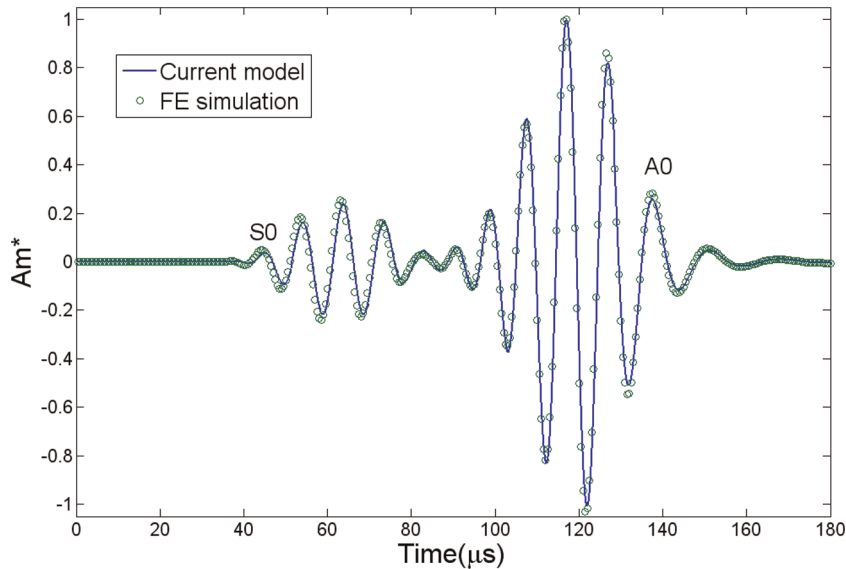


Figure 4. The transient guided wave response in the prestressed plate at $x = 226.5$ mm away from the piezo-actuator under excitation $f_c = 100$ kHz ($\sigma^0 = 0.8\sigma_Y$). FE: finite element.

where $\sigma^0 = 0.8\sigma_Y$, and the normalized Young's modulus of the host plate is $E^* = E/E_0$ with $E_0 = 79$ GPa. The excitation frequency is selected to be $f_c = 150$ kHz. As observed in Figure 6, the softer the host structural material is, the more prestress-induced variation in the wave velocity can be found for both GW modes. For example, the effects of the prestress on the GW-based SHM may become more profound for the aerospace

structures made of aluminum alloys ($E^* = 1.0$) than those made of high-strength steels ($E^* > 1.6$).

Tuned GW generation

The technique of wave frequency tuning, which can generate the strong desired GW mode sensitive to specific damages, has been widely used for GW inspection

of plate structures (Gangadharan et al., 2009; Giurgiutiu, 2005; Nieuwenhuis et al., 2005; Raghavan and Cesnik, 2005; Yu et al., 2010). However, no investigations have been reported to consider the effects of the prestress upon GW mode-tuning capabilities. Figure 7 demonstrates the normalized piezo-actuated responses of the fundamental S0 and A0 Lamb wave modes as a function of sweeping frequencies in the plate under various prestresses. In this figure, $\varepsilon_x^*(x, d)$ is the normalized surface strain along the x direction defined as the ratio of the surface strain with the prestress to that without the prestress. The actuator/host plate geometry parameters are $a/h = 20$ and $d/a = 0.333$. It can be observed that the overall shape of

wave-tuning curves is retained for both the S0 and A0 modes throughout the sweeping frequency under either pretension or precompression. The amplitude of the S0 mode is almost not affected by the applied prestress as shown in Figure 7(a), while the appearance of the pretension or the precompression can lead to an observable change in the wave amplitude and the tuning frequency shift of the A0 mode as shown in Figure 7(b). For example, compared with the case without prestress, around 15-kHz variation of tuning frequency for the first maximum A0 mode can be observed when the applied prestress reaches $0.8\sigma_Y$. Appropriate strategies need to be developed to compensate for the influences of the prestress (Croxford et al., 2007), such that

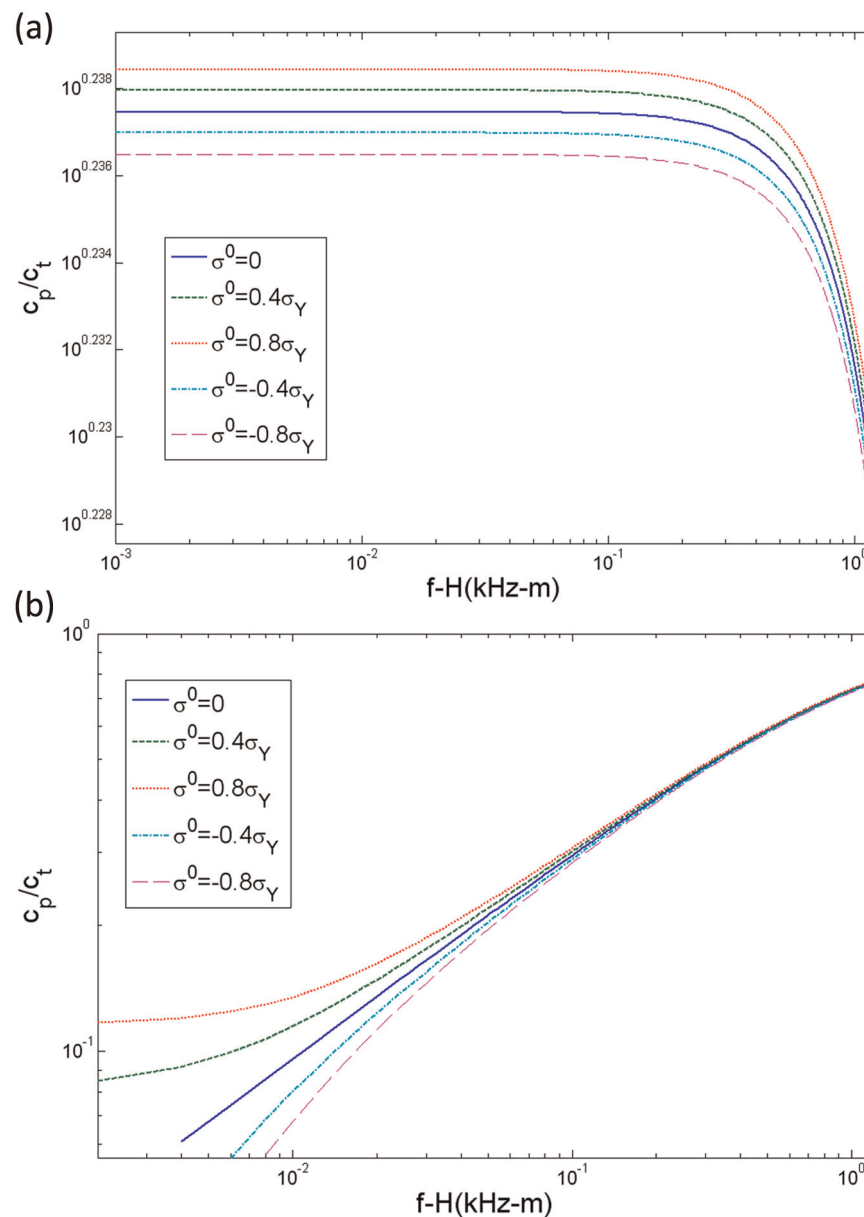


Figure 5. Phase velocities of Lamb wave propagation in an aluminum alloy plate under various prestresses: (a) the S0 mode and (b) the A0 mode.

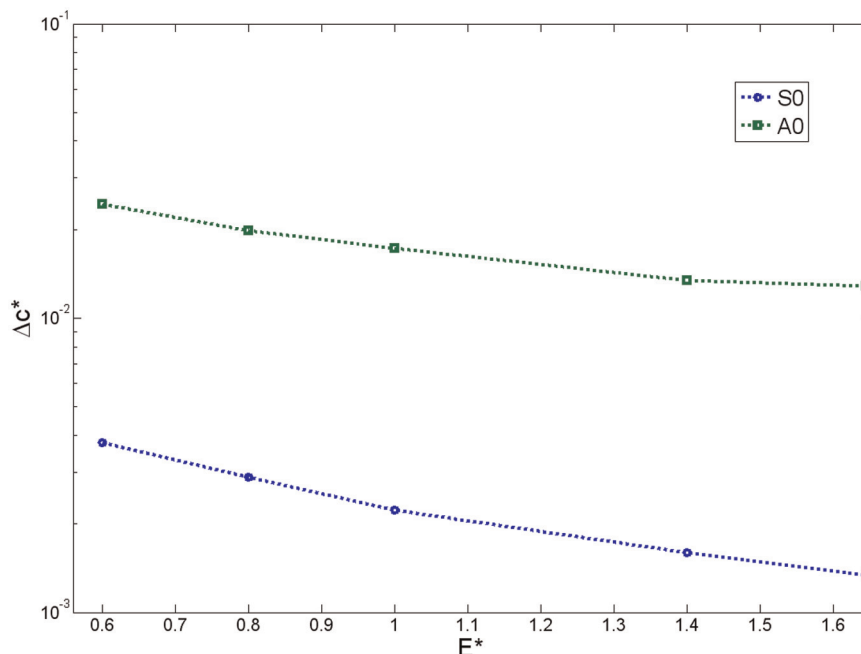


Figure 6. Effects of structural material properties on prestress-induced velocity variation of the guided wave modes.

the desired wave mode generation can be achieved to interrogate the prestressed structure.

Transient GW propagation

In practical GW-based SHM systems, the integrated piezo-actuators are often excited by narrow-band tone-burst signals to suppress the dispersion of the induced GWs, which is beneficial for further signal interpretation (Ihn and Chang, 2008). Based on the developed model, the GW signals excited by the piezo-actuator in the prestressed plate are evaluated. Figure 8 shows the transient piezo-actuated GW responses in the prestressed plate under different prestresses. The five-peak tone-burst signal (Song et al., 2012) at a central frequency of 150 kHz is used for excitation. The same material properties and geometrical parameters in Figure 7 are used for the host medium and the actuator. In Figure 8, $\epsilon_x^*(x, d)$ is the normalized surface strain along the x direction defined as the ratio of the surface strain with the prestress to that without the prestress. From Figure 8, it can be further substantiated that the S0 mode signal is not sensitive to the prestresses compared to the A0 mode, which is good for health monitoring of prestressed structures utilizing the S0 mode. In contrast, an obvious shift in the wave velocity and amplitude can be found for the A0 mode with varying prestresses, and such an observed shift has comparable magnitude to that caused by temperature variations (Lee et al., 2010; Raghavan and Cesnik, 2008). Similar effects of prestresses on piezo-actuated GW signals at higher frequency ($f_c = 400$ kHz) can be

seen in Figure 9, where the S0 mode is dominantly excited over the A0 mode. It is known that many signal-processing algorithms (e.g. using damage-induced scattered waves) are based on accurately measuring the wave velocity of the interrogative GW signals (Francis Rose and Wang, 2010; Michaels, 2008). Therefore, the influences of the prestress upon GW responses should be considered to obtain the calibrated diagnostic image of the structure, especially when the A0 mode is excited for damage detection in the prestressed structure.

According to the transient GW responses predicted by the current model, an appropriate SDC is proposed to quantitatively evaluate the overall change in the received GW signals caused by the prestress. The SDC, based on the root-mean-square change of the GW signals in the time domain (Michaels et al., 2011), is defined as

$$\text{SDC}(\sigma^0) = \sqrt{\frac{\sum_n [S(t_n, \sigma^0) - S(t_n, \sigma^0 = 0)]^2}{\sum_n [S(t_n, \sigma^0 = 0)]^2}} \quad (23)$$

where $S(t_n, \sigma^0)$ is the received transient GW signal at time t_n and the applied prestress σ^0 .

As an example, Figure 10 displays the normalized SDC for both GW modes as a function of applied prestresses, where SDC* represents the normalized value of SDC with respect to the maximum value. In the calculation, the excitation frequency is selected to be $f_c = 150$ kHz. It can be found, in Figure 10, that the

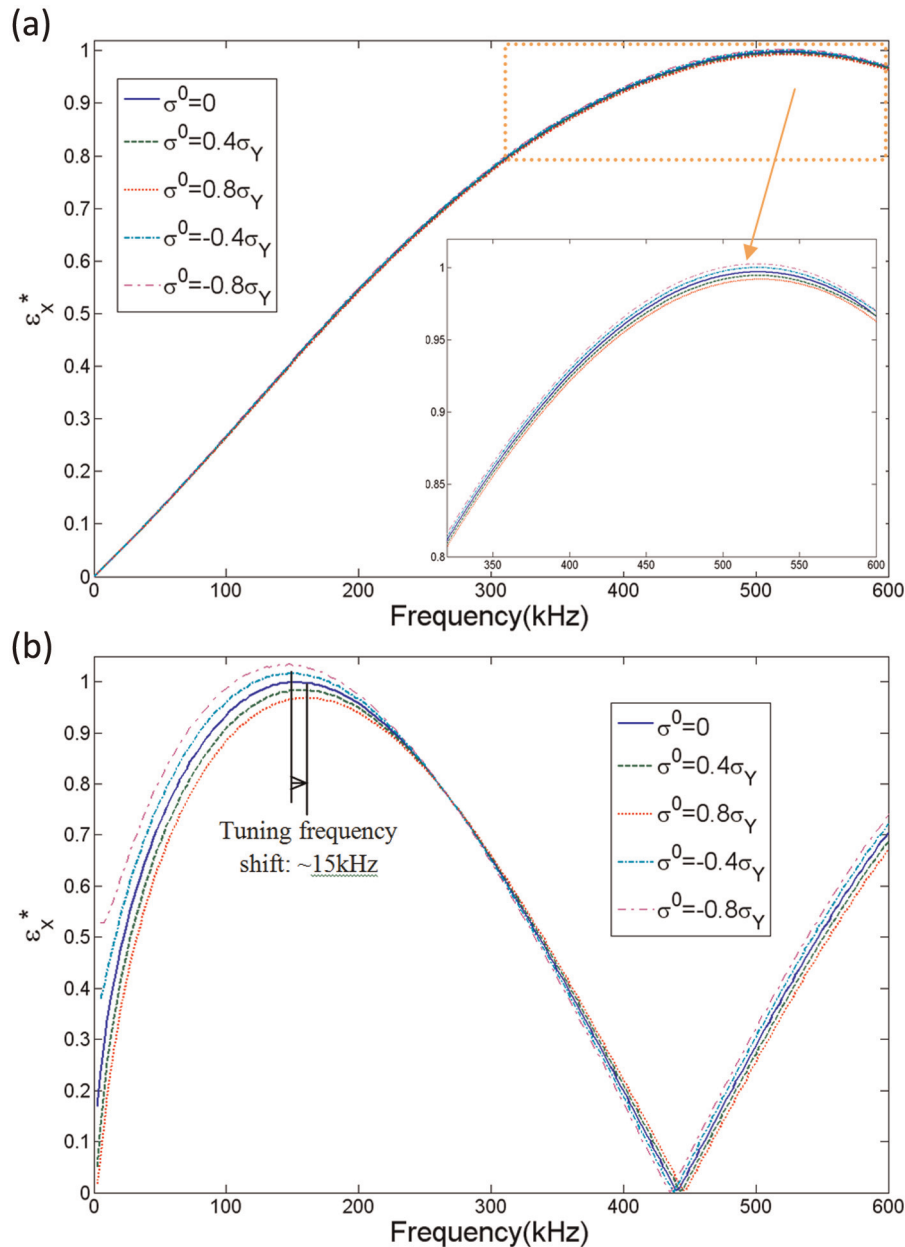


Figure 7. Piezo-actuated responses of the fundamental guided wave modes in a 2-mm thick aluminum alloy plate under various prestresses: (a) the S0 mode and (b) the A0 mode (actuator/host plate geometry: $a/h = 20$ and $d/a = 0.333$).

shape of the normalized SDC is approximately linear when the applied prestress is relatively small (e.g. $\sigma^0 < 0.2\sigma_Y$); however, the variation of the normalized SDC curve evidently exhibits some nonlinearity for the larger magnitude of the applied prestress especially for the A0 mode. Similar variation with respect to applied loads has been reported in a recent experiment study on load impact on the GW-based SHM (Michaels et al., 2011). Noticeably, most modern GW methods rely on scattered signals to identify small structural damage, which is often implemented by comparing received signals to baseline signals collected from the undamaged structure (Huang et al., 2010b; Lin and Yuan, 2005). If

the effects of the prestress on the GW-based SHM are neglected, however, those detection methods may most likely provide a false alarm or fail to diagnose in the presence of applied loads on the monitored structure.

Conclusion

In the study, we focus on the quantitative characterization of the GW generation and propagation in prestressed plate structures induced by the piezoelectric wafer. An analytical model considering coupled piezoelectrodynamics is first developed to study dynamic load transfer between a surface-bonded thin piezoelectric

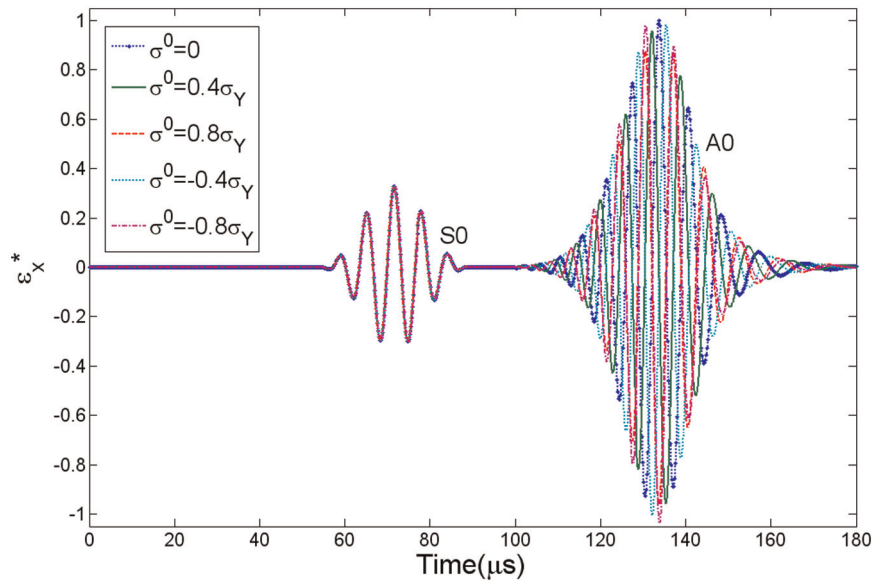


Figure 8. The transient guided wave responses at $x = 320.0$ mm away from the piezo-actuator at a central frequency of $f_c = 150$ kHz collected from the aluminum alloy plate submitted to different prestresses.

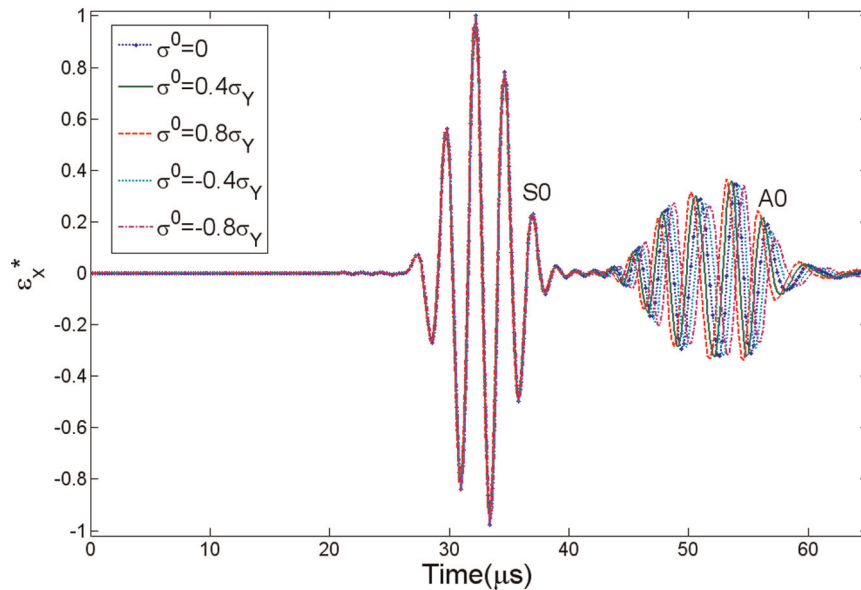


Figure 9. The transient guided wave responses at $x = 150$ mm away from the piezo-actuator at a central frequency of $f_c = 400$ kHz collected from the aluminum alloy plate submitted to different prestresses.

actuator and a prestressed plate. The accuracy of the analytical prediction is then evaluated through the comparison with the FE analysis. Based on the current model, the effects of the prestress on the GW propagation and mode-tuning capabilities are investigated at different frequencies for different host materials. Specifically, it is found that (1) the presence of the applied prestress can result in the observable variation in the wave amplitude and the tuning frequency shift of the A0 mode, and very little for the S0 mode; (2) for the softer host material under the applied prestress, the

variation in the wave velocity becomes more profound; and (3) the normalized SDC curve shows some non-linear variation with respect to the applied prestress especially for the A0 mode. This study can provide a theoretical base for on-line piezo-GW-based health monitoring of the prestressed aerospace structures.

Funding

This research was partly supported by National Natural Science Foundation of China under Grants No. 10832002 and NASA EPSCoR RID grant.

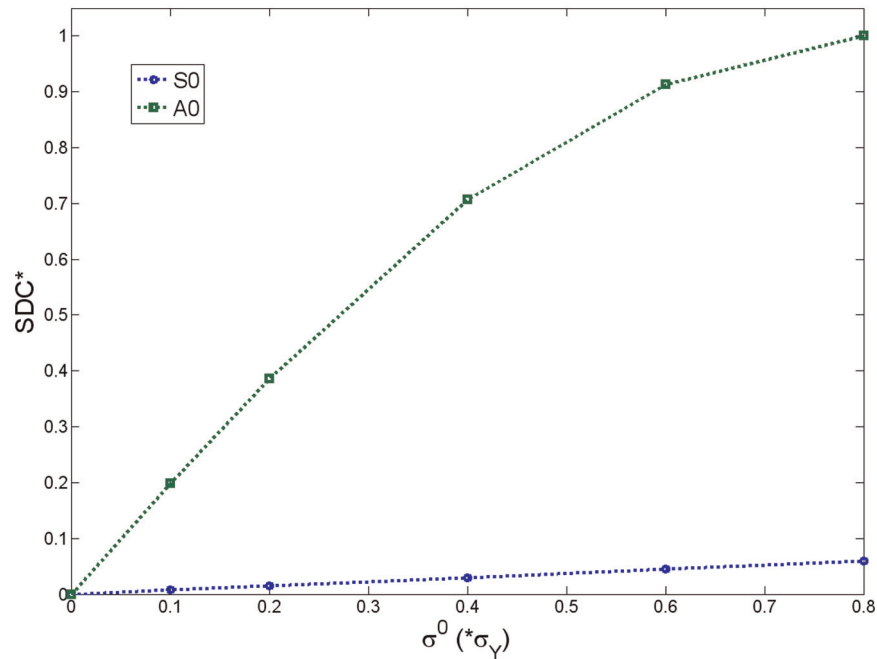


Figure 10. SDC* for the guided-wave responses as a function of the applied prestresses.
SDC*: normalized signal difference coefficients.

References

- Akbarov SD (2007) Recent investigations on dynamic problems for an elastic body with initial (residual) stresses (review). *International Applied Mechanics* 43: 1305–1324.
- An Y-K and Sohn H (2010) Instantaneous crack detection under varying temperature and static loading conditions. *Structural Control and Health Monitoring* 17: 730–741.
- Anton SR, Inman DJ and Park G (2009) Reference-free damage detection using instantaneous baseline measurement. *American Institute of Aeronautics and Astronautics Journal* 47: 1952–1964.
- Chen F and Wilcox PD (2007) The effect of load on guided wave propagation. *Ultrasonics* 47: 111–122.
- Crawley EF and De Luis J (1987) Use of piezoelectric actuators as elements of intelligent structures. *American Institute of Aeronautics and Astronautics Journal* 25: 1373–1385.
- Croxford AJ, Wilcox PD, Drinkwater BW, et al. (2007) Strategies for guided wave structural health monitoring. *Proceedings of the Royal Society A: Mathematical, Physical and Engineering Sciences* 463: 2961–2981.
- Desmet C, Kawald U, Mourad A, et al. (1996) The behavior of Lamb waves in stressed polymer foils. *Journal of the Acoustic Society of America* 100: 1509–1513.
- Doyle D, Zagrai A, Arritt B, et al. (2010) Damage detection in bolted space structures. *Journal of Intelligent Material Systems and Structures* 21: 251–264.
- Dugnani R (2009) Dynamic behavior of structure-mounted disk-shape piezoelectric sensors including the adhesive layer. *Journal of Intelligent Material Systems and Structures* 20: 1553–1564.
- Francis Rose LR and Wang CH (2010) Mindlin plate theory for damage detection: imaging of inhomogeneities. *Journal of the Acoustic Society of America* 127: 754–763.
- Fromme P and Sayir MB (2002) Measurement of scattering of a Lamb wave by a through hole in a plate. *Journal of the Acoustic Society of America* 111: 1165–1170.
- Gangadharan R, Murthy CRL, Gopalakrishnan S, et al. (2009) Time reversal technique for health monitoring of metallic structure using Lamb waves. *Ultrasonics* 49: 696–705.
- Giurgiutiu V (2005) Tuned Lamb wave excitation and detection with piezoelectric wafer active sensors for structural health monitoring. *Journal of Intelligent Material Systems and Structures* 16: 291–305.
- Giurgiutiu V (2008) *Structural health monitoring with piezoelectric wafer active sensors*. Amsterdam and Boston, MA: Elsevier Academic Press.
- Giurgiutiu V and Santoni GB (2009) Extension of the shear-lag solution for structurally attached ultrasonic active sensors. *American Institute of Aeronautics and Astronautics Journal* 47: 1980–1983.
- Glushkov E, Glushkova N, Kvasha O, et al. (2007) Integral equation based modeling of the interaction between piezoelectric patch actuators and an elastic substrate. *Smart Materials and Structures* 16: 650–664.
- Han L, Wang XD and Zuo M (2009) The dynamic behavior of a surface bonded piezoelectric actuator with a bonding layer. *Acta Mechanica* 206: 193–205.
- Hu YT, Yang JS and Jiang Q (2002) A model of electroelastic plates under biasing fields with applications in buckling analysis. *International Journal of Solids and Structures* 39: 2629–2642.
- Huang GL, Song F and Reddy R (2010a) Quantitative modeling of dynamic behavior of a piezoelectric wafer actuator bonded to an elastic plate for guided wave propagation. In: *Proceedings of SPIE health monitoring of structural and biological systems*, April 2008, San Diego, CA.

- Huang GL, Song F and Wang XD (2010b) Quantitative modeling of coupled piezo-elastodynamic behavior of piezoelectric actuators bonded to an elastic medium for structural health monitoring: a review. *Sensors* 10: 3681–3702.
- Huang GL and Sun CT (2006) The dynamic behavior of a piezoelectric actuator bonded to an anisotropic elastic medium. *International Journal of Solids and Structures* 43: 1291–1307.
- Ihn JB and Chang F-K (2008) Pitch-catch active sensing methods in structural health monitoring for aircraft structures. *Structural Health Monitoring* 7: 5–19.
- Jin C and Wang XD (2011) The effect of adhesive layers on the dynamic behavior of surface-bonded piezoelectric sensors with debonding. *Journal of Intelligent Material Systems and Structures* 22: 655–670.
- Karami G, Grundman N, Abolfathi N, et al. (2008) Thermal elastic characterization and evaluation of residual stresses in bi-directional fibrous composites. *Applied Composite Materials* 15: 259–272.
- Kundu T and Maslov K (1997) Material interface inspection by Lamb waves. *International Journal of Solids and Structures* 34: 3885–3901.
- Kwun H, Bartels KA and Hanley JJ (1998) Effects of tensile loading on the properties of elastic-wave propagation in a strand. *Journal of the Acoustic Society of America* 103: 3370–3375.
- Lanza di Scalea F and Salamone S (2008) Temperature effects in ultrasonic Lamb wave structural health monitoring systems. *Journal of the Acoustic Society of America* 124: 161–174.
- Lee SJ, Gandhi N, Michaels JE, et al. (2010) Comparison of the effects of applied loads and temperature variations on guided wave propagation. *AIP Conference Proceedings* 1335: 175–182.
- Lesieutre GA (2009) How membrane loads influence the modal damping of flexural structures. *American Institute of Aeronautics and Astronautics Journal* 47: 1642–1646.
- Lin X and Yuan F-G (2005) Experimental study applying a migration technique in structural health monitoring. *Structural Health Monitoring* 4: 341–353.
- Liu H, Kuang ZB and Cai ZM (2003) Propagation of Bleustein-Gulyaev waves in a prestressed layered piezoelectric structure. *Ultrasonics* 41: 397–405.
- Loveday PW (2009) Semi-analytical finite element analysis of elastic waveguides subjected to axial loads. *Ultrasonics* 49: 298–300.
- Michaels JE (2008) Detection, localization and characterization of damage in plates with an in situ array of spatially distributed ultrasonic sensors. *Smart Materials and Structures* 17: 035035.
- Michaels JE, Lee SJ and Michaels TE (2011) Impact of applied loads on guided wave structural health monitoring. *AIP Conference Proceedings* 1335: 1515–1522.
- Nieuwenhuis JH, Neumann JJ Jr, Greve DW, et al. (2005) Generation and detection of guided waves using PZT wafer transducers. *IEEE Transactions on Ultrasonics, Ferroelectrics* 52: 2103–2111.
- Park S, Anton SR, Kim JK, et al. (2010) Instantaneous baseline structural damage detection using a miniaturized piezoelectric guided waves system. *KSCSE Journal of Civil Engineering* 14: 889–895.
- Raghavan A and Cesnik CES (2005) Finite-dimensional piezoelectric transducer modeling for guided wave based structural health monitoring. *Smart Materials and Structures* 14: 1448–1461.
- Raghavan A and Cesnik CES (2007) Review of guided wave-structural health monitoring. *Shock and Vibration Digest* 39: 91–114.
- Raghavan A and Cesnik CES (2008) Effects of evaluated temperature on guided wave structural health monitoring. *Journal of Intelligent Material Systems and Structures* 19: 1383–1398.
- Ratwani MM (2000) Repair options for airframes. In: *Aging aircraft fleets—structural and other subsystem aspects*, Sofia, Bulgaria, AGARD Lecture Series 218.
- Santus C and Tayler D (2009) Physically short crack propagation in metals during high cycle fatigue. *International Journal of Fatigue* 31: 1356–1365.
- Senesi M and Ruzzene M (2011) A frequency selective acoustic transducer for directional Lamb wave sensing. *Journal of the Acoustic Society of America* 130: 1899–1907.
- Singh B (2010) Wave propagation in a prestressed piezoelectric half space. *Acta Mechanica* 211: 337–344.
- Song F, Huang GL and Hudson K (2009) Guided wave propagation in honeycomb sandwich structures by using a piezoelectric actuator/sensor system. *Smart Materials and Structures* 18: 125007.
- Song F, Huang GL and Hu GK (2012) On-line guided wave based debonding detection in honeycomb sandwich structures. *American Institute of Aeronautics and Astronautics Journal* 50: 284–293.
- Su J, Kuang ZB and Liu H (2005) Love wave in ZnO/SiO₂/Si structure with initial stresses. *Journal of Sound and Vibration* 286: 981–999.
- Tiersten HF, Sinha BK and Meeker TR (1981) Intrinsic stress in thin films deposited on anisotropic substances and its influence on the natural frequencies of piezoelectric resonators. *Journal of Applied Physics* 52: 5614–5624.
- Wang J, Wu RX, Du JK, et al. (2007) Effect of initial stresses on surface acoustic waves propagating in infinite elastic plates. In: *IEEE international frequency control symposium*, May, Geneva, Switzerland.
- Wang XD and Huang GL (2001) Wave propagation in electromechanical structures: induced by surface-bonded piezoelectric actuators. *Journal of Intelligent Material Systems and Structures* 12: 105–115.
- Yang J (2005) Free vibrations of an electroelastic body under biasing fields. *IEEE Transactions on Ultrasonics, Ferroelectrics* 52: 358–364.
- Yu Y, Santoni GB and Giurgiutiu V (2010) Shear lag solution for tuning ultrasonic piezoelectric wafer active sensors with applications to Lamb wave array imaging. *International Journal of Engineering Science* 48: 848–861.
- Von Ende S and Lammering R (2007) Investigation on piezoelectrically induced Lamb wave generation and propagation. *Smart Materials and Structures* 16: 1802–1809.
- Zagrai A, Doyle D, Gigineishvili V, et al. (2010) Piezoelectric wafer active sensor structural health monitoring of space structures. *Journal of Intelligent Material Systems and Structures* 21: 921–940.

Appendix I

Determination of the resulting initial stress

When a static stress σ^0 is initially applied on the host plate, the actuator is submitted to the resulting axial initial stress $\hat{\sigma}^0$. Based on the assumptions in the subsection ‘Modeling of the prestressed piezoelectric actuator,’ the actuator can be modeled as an electroelastic line subjected to the distributed axial load τ^0/h , and the equilibrium equation of the actuator along the axial direction can be then written as

$$\frac{d\hat{\sigma}^0}{dx} + \frac{\tau^0(x)}{h} = 0. \quad (24)$$

Since the load transferred between the actuator and the host plate can be attributed to τ^0 , the two ends of the actuator can be assumed to be traction free, that is

$$\hat{\sigma}^0 = 0, \quad |x| = a \quad (25)$$

By integrating equation (24) and making use of equation (25), the axial stress in the actuator can be expressed in terms of the shear stress τ^0 as

$$\hat{\sigma}^0(x) = - \int_{-a}^x \frac{\tau^0(\xi)}{h} d\xi, \quad |x| = a \quad (26)$$

with

$$\int_{-a}^a \tau^0(\xi) d\xi = 0 \quad (27)$$

The relation between the axial initial stress ($\hat{\sigma}^0$), strain ($\hat{\varepsilon}^0$), and the electric fields (\hat{E}^0) of this actuator model can be obtained by using the following general constitutive relation

$$\hat{\sigma}^0 = E_a \hat{\varepsilon}^0 - e_a \hat{E}^0 \quad (28)$$

where E_a and e_a are the effective elastic and piezoelectric material constants, $E_a = c_{11} - c_{13}^2/c_{33}$ and

$e_a = e_{13} - e_{33}c_{13}/c_{33}$, respectively, with c_{ij} and e_{ij} ($i, j = 1, 3$) being the components of the piezoelectric elastic stiffness matrix for a constant electric potential, and the piezoelectric constant matrix, respectively. In the initial static deformation, $\hat{E}^0 = 0$ is assumed. The resulting initial axial strain can then be obtained in terms of τ^0 as

$$\hat{\varepsilon}^0(x) = - \int_{-a}^x \frac{\tau^0(\xi)}{hE_a} d\xi, \quad |x| < a \quad (29)$$

The stress field produced inside the host plate can be caused by both the initial stress applied on the host plate with a traction free boundary and the surface shear stress τ^0 resulted from the actuator. The strain induced by τ^0 can be obtained by using the boundary condition along the top surface as

$$\sigma_{xz}^0(x, d) = -\tau^0(x), \quad |x| < a \quad \text{and} \quad \sigma_{zz}^0(x, d) = 0 \quad (30)$$

Making use of the quasi-static fundamental solution of an elastic plate subject to a tangential traction and following a similar manner as described in Huang et al. (2010a), the strain $\tilde{\varepsilon}_x^0$ resulting from the applied traction (equation (30)) can be determined in terms of the static interfacial shear stress τ^0 . Together with the constant strain $\varepsilon^0 = \sigma^0/E$ applied along the x direction at infinity, the total surface strain in the host plate can then be found by superimposing the solutions of both parts as $\varepsilon_x^0(x, d) = \tilde{\varepsilon}_x^0 + \varepsilon^0$.

The continuity of deformation between the actuator and the host medium indicates that

$$\varepsilon_x^0(x, d) = \hat{\varepsilon}^0, \quad |x| < a \quad (31)$$

Expanding τ^0 in terms of Chebyshev polynomials and following a similar procedure with the ‘Dynamic load transfer and resulting GW propagation’ subsection, the static interfacial shear stress τ^0 can be solved. Therefore, based on equation (26), the axial stress $\hat{\sigma}^0(x)$ in the actuator can be obtained.